Published in final edited form as:
J Proteome Res. 2011 August 5; 10(8): 3743–3754. doi:10.1021/pr200360w.

NMR Analysis of a Stress Response Metabolic Signaling Network

Bo Zhang[1], **Steven Halouska**[1], **Charles E. Schiaffo**[1], **Marat R. Sadykov**[2], **Greg A. Somerville**[2], and **Robert Powers**[1,*]

[1]Department of Chemistry, University of Nebraska-Lincoln Lincoln, NE 68588-0304

[2]School of Veterinary Medicine and Biomedical Sciences, University of Nebraska-Lincoln Lincoln, NE 68588-0905

Abstract

We previously hypothesized that *Staphylococcus epidermidis* senses a diverse set of environmental and nutritional factors associated with biofilm formation through a modulation in the activity of the tricarboxylic acid (TCA) cycle. Herein, we report our further investigation of the impact of additional environmental stress factors on TCA cycle activity and provide a detailed description of our NMR methodology. *S. epidermidis* wild-type strain 1457 was treated with stressors that are associated with biofilm formation, a sub-lethal dose of tetracycline, 5% NaCl, 2% glucose and autoinducer-2 (AI-2). As controls and to integrate our current data with our previous study, 4% ethanol stress and iron-limitation were also used. Consistent with our prior observations, the effect of many environmental stress factors on the *S. epidermidis* metabolome was essentially identical to the effect of TCA cycle inactivation in the aconitase mutant strain 1457-*acnA::tetM*. A detailed quantitative analysis of metabolite concentration changes using 2D ^{1}H-^{13}C HSQC and ^{1}H-^{1}H TOCSY spectra identified a network of 37 metabolites uniformly affected by the stressors and TCA cycle inactivation. We postulate that the TCA cycle acts as the central pathway in a metabolic signaling network.

Keywords

NMR; metabolomics; central metabolism; bioinformatics; stress response

Introduction

In eukaryotic organisms, signaling pathways are essential to the life-cycle of cells and are ubiquitous processes that regulate a variety of functions in response to both extracellular and intracellular environmental changes.[1–4] These signaling systems are spatially and temporarily organized, where the kinetic properties of these cycles depends on the cellular distribution of the activator and deactivator proteins. Protein activity is usually controlled through a variety of post-translational modifications (phosphorylation, acetylation, ubiquitylation, etc.), through protein complex formation, through transcription regulation, or

*To whom correspondence should be addressed: Robert Powers, Department of Chemistry, 722 Hamilton Hall, University of Nebraska, Lincoln, NE 68588-0304, Tel: (402) 472-3039; Fax (402) 472-9402, rpowers3@unl.edu.

Supporting Information

Supporting Information Available: Annotated S-plots and loading plots from the OPLS-DA analysis presented in Figures 2, 3 and 4. 3D versions of the 2D PCA scores plots presented in Figures 2, 3 and 4. The results, 2D PCA scores plot and metabolomic tree diagram for the effect of autoinducer-2 (AI-2) on the *S. epidermidis* metabolome. This material is available free of charge via the Internet at http://pubs.acs.org.

any combination of these factors. A prototypical signaling cascade includes a membrane-bound receptor that binds a signal molecule which in turn activates a kinase proximal to the membrane. This activated kinase phosphorylates a second kinase, where the cascade continues and perpetuates the signal away from the membrane to the final target. Typically, the impact of a signaling network is the up- and down-regulation of a set of genes or proteins associated with a specific response (apoptosis, metabolic process, proliferation, stress responses, etc.). Correspondingly, the cell commits a significant amount of energy and resources to undergo such a phenotype change.

In prokaryotes, signal transduction frequently involves two-component regulatory systems that consist of a membrane-bound sensor histidine protein kinase and a response regulator.[5] These two-component signal transduction systems are activated when an external signaling molecule, peptide, metal ion, etc., is bound by the sensor kinase, which undergoes autophosphorylation at a conserved histidine. Transfer of the phosphoryl group to the receiver domain of a response regulator in the cytoplasm of a bacterium completes the activation and the response regulator is then competent to activate transcription of a limited set of genes. In staphylococci, there are numerous two-component regulatory systems,[6] with the best studied being the *agr* quorum sensing system.[7] In addition to two-component systems, bacteria use sigma factors as a means to detect environmental conditions that induce heat stress, envelope stress, nitrogen stress, etc.[8] In staphylococci, σ^B is activated during stress conditions, growth phase transitions, and morphological changes.[9, 10] Most recently, the hypothesis that central metabolism can act as a signal transduction pathway to transduce external environmental signals (*e.g.*, iron-limitation) into intracellular metabolic signals by altering the activity of the enzymes of central metabolism has been proposed.[11]

The tricarboxylic acid (TCA) cycle is part of central metabolism and provides reducing potential, energy and biosynthetic intermediates necessary for other macromolecular synthesis.[12] Several studies have also shown that the TCA cycle is involved in regulating or affecting virulence or virulent determinant biosynthesis.[13–15] One specific example is the production of the exopolysaccharide, polysaccharide intercellular adhesion (PIA),[16] which is associated with virulence and biofilm formation.[17–20] PIA synthesis is regulated by nutrient availability and external stress conditions.[21, 22] Importantly, TCA cycle activity has also been shown to be affected by changes in environmental stress factors.[16, 22, 23] A number of environmental stress factors have also been shown to influence biofilm formation: ethanol,[24] oleic acid,[25] glucose,[26] UDP-N-acetylglucosamine,[27] sub-inhibitory concentrations of some antibiotics,[28] anaerobic conditions,[29] Fe limitation,[30–32] high osmolarity,[33] and high temperature.[33] The diversity of these external stimuli suggests a versatile regulation system. Recently, we used NMR metabolomics to demonstrate that Fe limitation and ethanol decrease TCA activity.[23] These stressors cause a common metabolic change that can be sensed by metabolite responsive-regulators (*e.g.*, catabolite control protein A; CcpA) that affect PIA production. We proposed that the TCA cycle plays a central role in a metabolic signaling network that senses disparate environmental stress conditions and regulates PIA biosynthesis, virulence determinants and biofilm formation (Figure 1). Herein, we report a further NMR analysis of the impact on the metabolome of *S. epidermidis* resulting from a diverse range of environmental stress factors associated with biofilm formation that include 5% NaCl,[33] 2% glucose,[26] 0.06 μg/mL tetracycline,[28] and 400 nM autoinducer-2 (AI-2, furanosyl borate diester),[34] in addition to our prior study[23] with 4% ethanol,[24] and Fe limitation.[30–32]

Our differential NMR metabolomics methodology has been applied to the study of *in vivo* drug activity in *Aspergillus nidulans*[35] and *Mycobacterium smegmatis*[36] and is ideally suited to a systems biology analysis of the impact of environmental stress factors on the *S. epidermidis* metabolome and the corresponding role of the TCA cycle.[23] In the latter study,

NMR was used to detect metabolic perturbations by following changes to *S. epidermidis* (strain 1457) cultured under environmental stress conditions that induce biofilm formation. These results were then compared to the metabolome of a *S. epidermidis* mutant (aconitase mutant strain SE1457-*acnA::tetM*) with an inactivated TCA cycle. If *S. epidermidis* senses environmental stress conditions by affecting TCA cycle activity as previously observed, then the impact on the metabolome caused by the aconitase mutant and the disparate external signals were expected to be equivalent. The overlapping clusters in principal component analysis (PCA) and orthogonal partial least squares discriminant analysis (OPLS-DA) two dimensional (2D) scores plot and the branch similarity on a metabolic tree diagram[37] indicate that external biofilm signals inactivate the TCA cycle. Furthermore, a detailed analysis of the relative concentration changes of 55 different metabolites from 2D ^{1}H-^{1}H TOCSY and 2D ^{1}H-^{13}C HSQC spectra implies the TCA cycle plays a central role in a metabolic signaling network.[35, 36, 38, 39] A metabolic network created with Cytoscape[40] illustrates this metabolic signaling network and the interrelationship of the TCA cycle activity with alanine metabolism, amino sugar metabolism, glycolysis/gluconeogenesis and the urea cycle.

Methods and Materials

Bacterial growth and NMR sample preparation

Staphylococcus epidermidis wild-type strain 1457 and the isogenic aconitase mutant strain 1457-*acnA::tet*M were grown in tryptic soy broth (TSB; BD Biosciences) without dextrose and supplemented with 0.25% glucose (Sigma Chemical) or 0.25% $^{13}C_6$-glucose (Cambridge Isotope Laboratories).

All bacterial cultures were inoculated to an optical density at 600 nm ($O.D._{600}$) of 0.06 and were grown for 2 hours or 6 hours at 37°C with 225 rpm aeration in TSB or TSB supplemented with a stressor know to induce biofilm formation. Either 10 or 12 replicate bacterial cultures were grown for each bacterial strain or environmental condition for the one-dimensional (1D) ^{1}H NMR experiments. 3 replicate bacterial cultures were grown for each bacterial strain or environmental condition for both the two-dimensional (2D) ^{1}H-^{13}C HSQC and the 2D ^{1}H-^{1}H TOCSY experiments.

In general, four different bacterial cultures were harvested per experiment: (1) wild-type *S. epidermidis* in TSB media, (2) wild-type *S. epidermidis* in TSB media with an environmental stress condition, (3) aconitase mutant of *S. epidermidis* in TSB, and (4) aconitase mutant of *S. epidermidis* in TSB with an environmental stress condition. The environmental stress conditions used in this study were 5% NaCl,[33] 2% glucose,[26] 0.06 μg/mL tetracycline,[28] 400 nM autoinducer-2 (AI-2, furanosyl borate diester)[34] in TSB media. To facilitate integrating this current work with our recent study,[23] control cultures containing 4% ethanol[24] in TSB or TSB medium depleted of iron (DTSB, defferated TSB)[30–32] were included for comparison. DTSB was prepared as described.[23] AI-2, furanosyl borate diester, was synthesized as previously described.[41, 42]

For the 1D ^{1}H NMR experiments, 2.74 $O.D._{600}$ units were harvested for analysis and for both the 2D ^{1}H-^{13}C HSQC and 2D ^{1}H-^{1}H TOCSY experiments 5.48 $O.D._{600}$ units were harvested. Following harvest, the culture medium was removed and the bacteria were suspended in 1 mL portions of 50 mM phosphate buffer (PBS) in 99.8% D_2O (Isotec) at pH 7.2 (uncorrected). The bacteria were lysed using a FAST-Prep instrument (MP Biomedicals) for 40 seconds, centrifuged for 5 min to remove the bacterial debris and glass beads, and frozen in liquid nitrogen.

NMR Data Collection

The NMR spectra were collected on a Bruker 500 MHz Avance spectrometer equipped with a triple-resonance, Z-axis gradient cryoprobe. A BACS-120 sample changer with Bruker Icon software was used to automate the NMR data collection. 1D ^{1}H NMR spectra were collected using excitation sculpting[43] to efficiently remove the solvent and maintain a flat baseline, eliminating any need for baseline collection that may induce artifacts in the PCA or OPLS-DA 2D or three-dimensional (3D) scores plot. 1D ^{1}H NMR spectra were collected at 298K with a spectrum width of 5482.5 Hz and 32K data points. A total of 16 dummy scans and 64 scans were used to obtain each spectrum.

2D ^{1}H-^{13}C HSQC spectra were collected with solvent pre-saturation and relaxation delay of 0.5 seconds.[44, 45] A total of 2048 data points with a spectrum width of 4734.9 Hz, and 128 data points with a spectrum width of 13834.3 Hz were collected in the ^{1}H and ^{13}C dimensions, respectively. A total of 8 dummy scans and 128 scans were used to obtain each of the 2D ^{1}H-^{13}C HSQC NMR spectra. 2D ^{1}H-^{1}H TOCSY spectra were collected with WATERGATE solvent pre-saturation, and a relaxation delay of 2 seconds.[46, 47] A total of 2048 data points with a spectrum width of 5000.0 Hz, and 256 data points with a spectrum width of 5001.3 Hz were collected in the direct and indirect ^{1}H dimensions, respectively. A total of 16 dummy scans and 8 acquisition scans were used to obtain each of the 2D ^{1}H-^{1}H TOCSY NMR spectra.

NMR Data Analysis

1D ^{1}H NMR spectra were processed in the ACD/1D NMR manager version 12.0 (Advanced Chemistry Development, Inc). The residual H_2O NMR resonance was removed. Intelligent bucketing was used to integrate each region with a bin size of 0.025 ppm. Each NMR spectrum was center averaged to minimize any experimental variations between bacterial cultures as follows:

$$Z=\frac{X_i-\overline{X}}{\sigma} \quad (1)$$

where $\bar{X}$ is the average signal intensity, σis the standard deviation in the signal intensity, and X_i is the signal intensity within a bin. Noise regions of the spectra were omitted from the PCA analysis by setting the corresponding bins to zero.[48] The table of integrals was imported into SIMCA11.0+ (UMETRICS) for PCA and OPLS-DA analysis using the program's standard parameters. The identification of the control group and treated group or groups for the OPLS-DA analysis was based on the PCA clustering pattern.

2D NMR Spectra were analyzed using NMRView[49] and Sparky (T. D. Goddard and D. G. Kneller, SPARKY 3, University of California, San Francisco) to identify chemical shifts and assign peak intensities. Peak intensities were normalized for each 2D NMR spectrum by dividing by the average peak intensity for a given spectrum. Each peak for each metabolite from each specific triplicate data set was averaged and the intensity for each peak was further normalized across all data sets (i.e., wild-type, aconitase mutant, and each bacterial growth condition). Specifically, the maximal intensity for each peak across all data sets was set to 100. The peak intensities in the remaining data sets were all scaled relative to this peak intensity. Then, a normalized intensity for the metabolite within each data set was calculated by averaging the normalized intensity for each of the metabolite's assigned peaks. In this manner, the relative percent difference in metabolite intensity (concentration) can be reported between different bacterial strains or bacterial growth conditions. As an illustrative example, consider a metabolite with thee assigned peaks (*A*, *B*, *C*) in a 2D ^{1}H-^{13}C HSQC spectrum. The 2D ^{1}H-^{13}C HSQC spectrum is collected in triplicate under three different

bacterial growth conditions for a total of 9 spectra and 27 peak intensities, 3 peaks in each spectrum for the metabolite. Peak *A* has average intensities of 0.05, 0.10, and 0.20 in the three different bacterial growth conditions, respectively. The values would be normalized to 25, 50, and 100. Similarly, peaks *B* and *C* are normalized against their maximal peak intensities for values of 20, 60, 100 and 30, 65, 100, respectively. Thus, the average relative concentrations of the metabolite under the three bacterial growth conditions would be the average of the three normalized peaks, yielding values of 25, 58.3 and 100, respectively. The bacterial growth condition with the highest relative metabolite concentration (100) would have a corresponding concentration increase of 75 and 41.7 relative to the two other bacterial growth conditions.

The observed NMR peaks in the 2D ^{1}H-^{13}C HSQC and 2D ^{1}H-^{1}H TOCSY spectra were assigned to specific metabolites using ^{1}H and ^{13}C chemical shift tolerances of 0.05 ppm and 0.50 ppm, respectively. Metabominer,[50] Madison Metabolomics Consortium Database (MMCD)[51], the BioMagResBank,[52] and Human Metabolome Database[53] were used to identify metabolites. The presence of metabolites and metabolic pathways were verified with the KEGG[54] and Metacyc[55] databases. A metabolic network map was generated using Cytoscape using a force directed layout.[40] Metabolites identified with a percent concentration difference of ≥ ±10% relative to wild-type *S. epidermidis* were manually color-coded to indicate either an up- or down-regulated concentration change.

Results and Discussion

NMR metabolomics and principle component analysis

The elimination of experimental factors that may inadvertently influence PCA or OPLS-DA metabolomic data interpretation is essential. The observed variability in the PCA or OPLS-DA data should result from differences in the biological samples as opposed to changes in sample preparation, sample handling, data acquisitions, data processing or any number of experimental parameters (temperature, pH, time, concentration, etc.). In order to obtain accurate and reproducible metabolomic data, the following general protocols were employed: (i) bacterial cultures of wild-type *S. epidermidis* were used as a reference metabolome and were prepared with all sets of bacterial cultures, (ii) equivalent bacterial numbers were used, so metabolite concentrations were independent of any bacterial growth variability, (iii) all NMR spectra were normalized using center averaging,[56] so variability in sample concentration was minimized, (iv) noise regions[48] and solvents were removed from NMR spectra prior to PCA or OPLS-DA, and (v) minimal processing (no baseline correction or apodization functions) of the NMR spectra.

Harvesting of S. epidermidis cultures

Bacteria grown in *vitro* undergo four different growth phases: (i) lag, (ii), exponential, (iii) stationary, and (iv) death. Throughout a typical growth cycle, the state of the bacteria and the environment are constantly changing. Clearly, there is a fundamental difference between the exponential phase, when cell density is relatively low, cells are rapidly dividing and the required nutrients are abundant; and the stationary phase when these characteristics are effectively reversed. Correspondingly, the metabolome is expected to reflect these differences. Therefore, exploring a biological system by monitoring changes in the metabolome necessitates the appropriate choice of the state of the system. In the case of *S. epidermidis* biofilm formation and the proposed role of the TCA cycle in a metabolic signaling network, the proper choice of the state of the system requires endogenous TCA cycle activity.

The TCA cycle is minimally active during the exponential phase (2 h growth) when nutrients (*i.e.*, glucose or other rapidly catabolizable carbohydrates) are sufficient for bacteria to grow quickly.[16, 57] Overflow metabolism results in an incomplete oxidation of glucose, leading to the accumulation of acetate, lactate, and other incompletely oxidized metabolites in the culture medium (Figure 2a). During the transition to the post-exponential growth phase (6 hours), the TCA cycle is de-repressed as the carbohydrate(s) are depleted from the culture medium. Concomitantly, the incompletely oxidized metabolites that accumulated in the medium are catabolized through the TCA cycle resulting in the depletion of secondary metabolites from the culture medium.

The growth phase-dependent activity of the TCA cycle in *S. epidermidis* is also apparent from the PCA 2D scores plot generated from 1D ^{1}H NMR spectra of *S. epidermidis* cell lysate (Figure 2b). The 2D PCA scores plot indicates that PC1 and PC2 account for 20.6% and 10.7% of the variations in the NMR spectra, respectively. A 3D PCA scores plot (Figure 1S) did not improve cluster separations. Each 1D ^{1}H NMR spectrum obtained for each cell lysate is represented as a single point in the PCA 2D scores plot, where the 10 replicates form four distinct clusters for the wild-type and aconitase mutant strains grown for 2 hours and 6 hours, respectively. As expected and consistent with our prior study,[23] the metabolomes of the *S. epidermidis* wild-type and aconitase mutant cells from the exponential growth phase (2 hours) were more similar to each other than the 6 hour cultures. This is apparent from the close clustering in the 2D scores plot for the 2 hour wild-type and aconitase mutant. This is consistent with the minimal activity of the TCA cycle at 2 hours and the loss of TCA cycle activity for the aconitase mutant. Conversely, there is a large separation in the 2D scores plot along the PC1 axis between the 6 hour wild-type and aconitase mutant. In fact, the 6 hour aconitase mutant cluster is closer to the 2 hour wild-type cluster. Again, this is consistent with an increase in TCA activity at 6 hours and the loss of TCA activity in the aconitase mutant. Correspondingly, the separation along PC1 reflects TCA cycle activity. Since the TCA cycle is minimally active during the exponential phase, the 2 hour wild-type cluster is slightly closer to the 6 hour wild-type cluster along PC1, compared to the aconitase mutants.

Alternatively, the separation along PC2 axis may reflect the variability in nutrients available to the cells. Glucose is still present after 2 hours of bacterial growth, but is being depleted while acetate is being accumulated. After 6 hours of growth, the depletion of acetate is dependent on TCA cycle activity, resulting in the largest separation along PC2 between the 6 hour aconitase mutant and the 2 hour wild-type samples. These two samples correspond to the largest expected variation in glucose and acetate concentrations. From the detailed 2D NMR analysis (*please see below*), acetate is approximately twice as concentrated in the 6 hour wild-type sample compared to the 2 hour aconitase mutant. The glucose concentration is effectively reversed. Glucose is twice as concentrated in the 2 hour aconitase mutant compared to the 6 hour wild type sample.

The PCA results were used to guide a subsequent analysis using OPLS-DA (Figure 2C). The OPLS-DA yielded a reliable model (R^2X 0.788, R^2Y 0.992, Q^2 0.992). The R^2 and Q^2 values represent the goodness of fit and predictability of the model, respectively. The OPLS-DA scores plot is similar to the PCA scores plot, except for the limited separation between the 2 hour wild-type and aconitase mutant clusters. Again, this is consistent with the minimal TCA activity expected for the 2 hour wild-type and aconitase mutant. Also, OPLS-DA emphasizes the difference between the control group (6 hour wild-type) and the treated classes, while minimizing contributions from within group variations. Thus, OPLS-DA generates significantly tighter clusters than PCA. More importantly, the S-plot and loading plot (Figure 2S) generated from the OPLS-DA provides unambiguous identification of the major contributors to the class separation (i.e., ^{1}H NMR bins and associated metabolites).

Specifically, comparing the 6 hour aconitase mutant and the 6 hour wild-type samples, which had the largest separation along PC1 in the PCA 2D scores plot, identified citrate, isocitrate, and other TCA related metabolites. Similarly, comparing the 2 hour aconitase mutant and the 2 hour wild-type samples, which had the largest separation along PC2 in the PCA 2D scores plot, identified glucose, acetate and other nutrients required for cell growth. These results provide strong support for our subjective analysis of the trends in the 2D PCA scores plot and demonstrate that not only does PCA and OPLS-DA differentiate between metabolic profiles, but they also provide information about specific enzymatic activity and environmental conditions.

Impact of environmental stress conditions on the S. epidermidis metabolome

Numerous genes and protein complexes are involved in the transformation of planktonic cells to a biofilm.[58] This process requires that *S. epidermidis* "sense" changes in its environment and the availability of nutrients, such as changes in temperature, O_2 levels, osmorality, ethanol, glucose and iron.[29, 31, 33, 59–63] It is reasonable to expect that different external factors would trigger distinct signaling pathways and mechanisms of biofilm regulation. Correspondingly, different biofilm formation pathways would presumably induce dissimilar metabolomic profiles. Alternatively, a versatile regulation system responsive to disparate signals would be significantly more efficient. A metabolic signaling pathway is one potential mechanism of rapidly responding to changing environmental stress conditions. Conceptually, the environmental flux of essential nutrients and metabolites would direct the up- or down- regulation of specific metabolic pathways in response to concentration changes (Le Chatelier's principle) to initially reestablish equilibrium without affecting protein activity. Effectively, a limited or abundant metabolite would direct the metabolic flow through a specific pathway causing a cascade affect due to the high interrelationship of the metabolome. Eventually, gene and protein regulation processes would respond to the perturbed metabolic activity leading to the up- or down- regulation of specific genes and proteins.

We have previously demonstrated that both Fe limitation and 4% ethanol decrease TCA cycle activity.[23] These environmental stress factors are known to induce *S. epidermidis* biofilm formation.[24, 30–32] We have also demonstrated that Fe limitation and 4% ethanol had a similar impact on the *S. epidermidis* metabolome and altered the activity of CcpA, a metabolite-responsive regulator. An important role for the TCA cycle in a staphylococcal biofilm metabolic signaling pathway seems apparent, especially since the TCA cycle is a central metabolic pathway that interacts with numerous other pathways (Figure 1). Thus, we proposed that the TCA cycle senses environmental stressors and transduces this signal through the metabolome to activate or repress the activity of metabolite-responsive regulators, which, in turn, modulates PIA production, virulence factor synthesis, and biofilm formation.[23] To further support our hypothesis that the TCA cycle senses disparate environmental signals to regulate PIA synthesis and biofilm formation, we analyzed changes in the *S. epidermidis* metabolome caused by additional environmental stress factors also known to induce an *S. epidermidis* biofilm.[2628, 33, 64]

S. epidermidis cultures were treated with 5% NaCl, 2% glucose, 0.06 μg/mL tetracycline, and 400 nM of autoinducer-2 (AI-2, furanosyl borate diester). Glucose and NaCl were reported to induce biofilm formation by the regulation of the *rbf* gene,[65] which has been shown to be a regulator of *icaR*,[66] a negative regulator of the *icaADBC* operon that is required for PIA synthesis and biofilm formation.[67] Subinhibitory concentrations of antibiotics enhance *icaADBC* gene expression[28, 68] by potentially inhibiting TcaR, a weak negative regulator of *icaADBC* gene expression.[69] AI-2 is an intercellular signaling molecule that has a modest effect on staphylococcal biofilms.[64] Conversely, if these additional environmental stress factors impact the *S. epidermidis* metabolome in a manner

similar to Fe limitation and 4% ethanol, which is also correlated with TCA cycle inactivation, then these results would further support the hypothesis that the TCA cycle acts as a signal transducer as a part of a metabolic signaling network.

The PCA 2D scores plot (Figure 3A) and the associated metabolic tree (Figure 3C) indicates that *S. epidermidis* wild-type cultures grown with the addition of the environmental stressors 4% ethanol, 0.06 μg/mL tetracycline or iron-limitation exhibited essentially identical metabolomes as the aconitase mutant. Both the aconitase mutant and wild-type cultures under these stress conditions formed a large cluster distinct from the cluster of wild-type cells in standard growth media. These results further support our hypothesis that environmental stress factors influence biofilm formation by inactivating the TCA cycle and re-directing key metabolites into PIA synthesis. Conversely, growing *S. epidermidis* wild-type cells in the presence of 5% NaCl showed no significant effect on the metabolome since the wild-type cells in the presence and absence of 5% NaCl cluster together. Similarly, AI-2 did not affect the *S. epidermidis* metabolome since both the wild-type and aconitase mutant cells in the presence and absence of 400 nM AI-2 cluster together (Figure 5S). Interestingly, *S. epidermidis* cells treated with 2% glucose were separated from both the wild-type and aconitase mutant clusters, implying a different impact on the metabolome and a unique mechanism of regulating biofilm formation. Alternatively, the addition of 2% glucose may be viewed as an intermediary effect, where the metabolome of the *S. epidermidis* cells grown with 2% glucose is moving toward the aconitase mutant cells. Effectively, the amount of glucose added to the bacterial culture was insufficient to completely inactivate the TCA cycle. It has been previously shown that different strains have different glucose uptake rates and different sensitivities to glucose-induced biofilm formation.[70, 71]

The PCA results were used to guide a subsequent analysis using OPLS-DA (Figure 3B) and the corresponding metabolomics tree diagram (Figure 3D). The OPLS-DA analysis yielded a reliable model (R^2X 0.637, R^2Y 0.966, Q^2 0.941), and results identical to PCA. The wild-type cells in the presence and absence of 5% NaCl were defined as the controls and, as expected, formed a single cluster in the 2D scores plot. *S. epidermidis* wild-type cultures grown with the addition of the environmental stressors 4% ethanol, 0.06 μg/mL tetracycline or iron-limitation again formed a single cluster with the aconitase mutant in the 2D OPLS-DA scores plot. Also similar to the PCA results, the *S. epidermidis* cells grown with 2% glucose formed a unique cluster. Thus, the corresponding metabolomics tree diagram identified three distinct clusters with bootstrap values of 100. The OPLS-DA results further support our hypothesis that environmental stress factors influence biofilm formation by inactivating the TCA cycle and re-directing key metabolites into PIA synthesis.

To verify the observed effect on the *S. epidermidis* metabolome is due to inactivating the TCA cycle as opposed to other potential factors, the *S. epidermidis* aconitase mutant strain was also grown with the addition of 4% ethanol, 0.06 μg/mL tetracycline, 2% glucose, 5% NaCl or under iron-limitation conditions. If the impact of these stress conditions is primarily through the inactivation of the TCA cycle, then the metabolome of the aconitase mutant strain should be unperturbed. Otherwise, if the stress conditions induce additional or alternative responses, then changes in the metabolome should be observed. The 2D PCA scores plot (Figure 4A) and metabolomic tree (Figure 4C) indicate the stress conditions did not affect the metabolome of the aconitase mutant. The aconitase mutant with and without the stress conditions forms a large cluster distinct from the wild-type cluster. Importantly, this includes the addition of 2% glucose. This implies the addition of 2% glucose to wild-type *S. epidermidis* resulted in an incomplete inactivation of the TCA cycle instead of a novel mechanism of biofilm regulation. Again, the PCA results were used to guide a subsequent analysis using OPLS-DA (Figure 4B) and the corresponding metabolomics tree diagram (Figure 4D). The OPLS-DA analysis yielded an acceptable model (R^2X 0.488, R^2Y

0.976, Q^2 0.961), and results very similar to PCA. The lower R^2X is consistent with the larger spread observed within the two primary clusters. The wild-type cells were defined as the controls and, as expected, the aconitase mutant with and without the stress conditions formed a single large cluster. Consistent with the PCA analysis, the single cluster also contained the addition of 2% glucose. The OPLS-DA scores plot, along with the metabolomics tree diagram, suggests sub-clusters are present within the large aconitase mutant cluster. But, the aconitase mutant data is spread throughout this cluster, such that an ellipse that corresponds to the 95% confidence limit for the aconitase mutant data encompasses the two other apparent sub-clusters. This result indicates that within the resolution of the PCA and OPLS-DA model, no statistical difference is observed between the metabolomes of the aconitase mutant with and without the stress conditions. Critically, the S-plot and loading plot obtained from the comparison between the wild-type cells and the aconitase mutant treated with the stress conditions was identical to the S-plot and loading plot generated from the comparison between the wild-type cells and the untreated aconitase mutant cells (Figures 3S,4S). Again, this supports the conclusion that the addition of the stressors did not perturb the metabolome of the aconitase mutant cells.

Detailed analysis of changes to the S. epidermidis metabolome caused by environmental stress

An overall correlation between the metabolomes of *S. epidermidis* under stress and TCA cycle inactivation provides further support for our hypothesis that environmental conditions induce biofilm formation though the regulation of the TCA cycle.[23] Specifically, the disparate signals of 2% glucose, 4% ethanol, 0.06 μg/mL tetracycline and iron-limitation are all sensed by the TCA cycle. To further support our hypothesis, a detailed analysis of changes to the *S. epidermidis* metabolome caused by these environmental stress factors was necessary. We previously reported an analysis of changes in the metabolome of *S. epidermidis* caused by TCA cycle inactivation that resulted in an increase in PIA production.[16] Among other observed changes, amino-acids derived from TCA cycle intermediates (Asn, Asp, Gln, and Glu) exhibited a decrease in concentration. Correspondingly, an increase in concentrations was observed for the PIA biosynthetic precursors UDP-N-acetyl-glucosamine and fructose-6-phosphate. A similar approach using 2D ^{1}H-^{13}C HSQC and 2D ^{1}H-^{1}H TOCSY NMR spectra was applied to quantitate metabolite changes in the *S. epidermidis* metabolome caused by Fe-limitation and 4% ethanol (Figure 5).[23]

2D NMR spectra improve metabolite identification by reducing the complexity and congestion of 1D ^{1}H NMR spectrum by spreading the information into two-dimensions. Additionally, the 2D ^{1}H-^{13}C HSQC experiment allows for monitoring the flow of carbon-13 through the metabolome from a specifically ^{13}C-labeled metabolite. Alternatively, the 2D ^{1}H-^{1}H TOCSY spectrum monitors all detectable metabolites with a bias to metabolites with the highest concentration. This may include the carbon-13 labeled metabolites observed in the 2D ^{1}H-^{13}C HSQC spectrum in addition to non-isotope labeled metabolites produced from other carbon sources. Therefore, the 2D ^{1}H-^{13}C HSQC and 2D ^{1}H-^{1}H TOCSY NMR spectra are complementary experiments for metabolomics and allow for a more complete analysis of metabolite concentration changes. Specifically, *S. epidermidis* wild-type cells and the aconitase mutant cells were grown with and without stress factors and harvested during either the exponential or post-exponential phase with and without the addition of ^{13}C-glucose. A total of 12 different bacterial culture conditions were prepared in triplicate for both the 2D ^{1}H-^{13}C HSQC and 2D ^{1}H-^{1}H TOCSY NMR experiments for a minimum of 72 bacterial cultures or NMR experiments. To maintain consistency, *S. epidermidis* wild-type cells were used as a reference and prepared with each bacterial culture set.

Differences in metabolite concentrations between the stresses, the bacterial growth phases, the aconitase mutant cells, and the wild-type cells was based strictly on detecting changes in peak intensities in the 2D ^{1}H-^{13}C HSQC and 2D ^{1}H-^{1}H TOCSY NMR experiments. To minimize contributions from experimental variability, three levels of normalization were used. First, metabolite concentrations were normalized based on the total number of cells grown for each culture. Second, the peak intensities in each NMR spectrum were normalized by the spectrum's average peak intensity. Third, each individual peak was normalized by scaling by the largest intensity observed for that peak across the set of NMR spectra. The intensity of peaks assigned to each metabolite within a spectrum were averaged and then averaged across the triplicate NMR data set. Relative changes in peak intensities (metabolite concentrations) were compared to the *S. epidermidis* wild type metabolome and are displayed as bar graphs in figure 6. Importantly, the metabolites identified from the 2D NMR experiments were also consistent with the metabolites identified as the major contributors to class distinction in the 2D OPLS-DA plots (Figures 3,4). The OPLS-DA S-plots and loading plots (Figure2 3S,4S) identifies the relative contribution of each bin (^{1}H NMR chemical shift) to the clustering in the corresponding 2D scores plot. Each NMR bin with a high reliability (p(corr)[1] ~ 1 or −1) and a high magnitude (p[1] > 0.1 or < −0.1) was assigned to a metabolite that was also found to be present in the figure 6 bar graph.

An inactivated TCA cycle caused concentration changes for 55 metabolites involved in the amino sugar pathway, glycolytic pathway, several amino acid pathways, and the TCA cycle. The NMR data shows the amount of cellular glucose in the 6 hour post-exponential wild-type strain was reduced by 80% compared to the 2 hour exponential phase. The amount of cellular acetate was increased by 25%. As expected, the inactivation of the TCA cycle in the aconitase mutant resulted in the accumulation of a large concentration of acetate. Acetate was the most intense peak in the 6 hour cultures for the wild-type and aconitase mutant strains shown in figure 5. There were also noticeable differences in the aconitase mutant metabolome. Peaks corresponding to the amino acids derived from the TCA cycle intermediates such as Asn, Asp, Gln, and Glu were not present. Not surprisingly, a large amount of citrate was also seen, since the inactivated aconitase prevents the conversion of citrate to isocitrate. Other metabolites associated with the glycolytic pathway were up-regulated. Similarly, some amino sugar and aromatic metabolites were up-regulated except for the significant down-regulation of UDP-glucuronate.

As expected from the clustering pattern in the 2D PCA scores plot, the direction of carbon flow in cells under stress were similar to the aconitase mutant cells, but dramatically different from wild-type cells during post exponential growth. A decrease in the concentration of amino acids derived from TCA cycle intermediates such as Asp, Asn, Glu, and Gln shows that the TCA cycle is still repressed when the cells are under stress. Instead the carbon flow is redirected back into the glycolytic pathway as indicated by an increase in concentrations for phosphoenolpyruvate (PEP), acetaldehyde, and fructose 6-phosphate. The carbon flow was also directed into the amino sugar pathway with an increase in concentrations for UDP-N-acetylglucosamine, N-acetyl-neuraminate, and N-acetyl-D-mannosamine. UDP-N-acetylglucosamine is an important precursor to PIA formation. Again, the detailed analysis of changes in the metabolome of *S. epidermidis* provides additional support for the role of TCA cycle activity in a metabolic signaling pathway that transduces disparate external stimuli into internal metabolic signals that facilitate biofilm formation. Effectively, the observed changes in the metabolome caused by disparate external stimuli are consistently suppressing TCA cycle activity and inducing PIA synthesis required for biofilms.

Conversely, the change of the carbon flow in the 2 hour growth is minimal. Again, this is consistent with the low TCA activity and the similar clustering in the 2D PCA scores plot

between the aconitase mutant and wild-type 2 hour growth (Figure 2b). Obviously, stress factors cannot suppress an already inactive TCA cycle. Instead, the catabolic conversion of glucose into intermediates throughout the glycolytic pathway proceeds as expected with a slight change since pyruvate is also produced. Much of the carbon-13 from glucose was still directed to the production of acetate. The NMR data indicates cellular acetate concentrations were similar across the 2 hour bacterial cultures, but an increased amount of acetyl-phosphate was accumulated under stress conditions. This confirms that when an abundant amount of glucose is present, it is processed by glycolysis and pyruvate dehydrogenase into acetyl-CoA and converted into acetyl-phosphate for use in substrate level phosphorylation. The excretion of acetate into the culture medium helps pH homeostasis due to the large flux of acetate.[72] Aside from the glycolytic pathway, the NMR data indicates that wild-type bacteria tend to utilize glucose more efficiency based on small decreases in amino sugar and aromatic metabolites.

Metabolic rearrangements during TCA cycle stress

The metabolome of *S. epidermidis* is not a series of independent isolated metabolic pathways, but instead is a complex inter-connected network. Thus, metabolic pathways connected to the TCA cycle are also affected by changes in TCA cycle activity. In order to visualize the cascade effect of inactivating the TCA cycle, a metabolic network was constructed using Cytoscape.[40] The metabolic network (Figure 7) was generated by manually associating each metabolite to its corresponding pathway from the KEGG[54] database and then using the automated biological network modules integrated into Cytoscape.[73, 74] The network connects the 37 metabolites identified by NMR whose concentrations are either increased (red) or decreased (green) by an inactivated TCA cycle. Only metabolites affected by a minimally active TCA cycle under all circumstances (aconitase mutant and stress factors) are highlighted on the network map. It is important to note that NMR is not able to identify every metabolite affected by perturbing the metabolome. The concentrations or stabilities of some metabolites are simply below the NMR detection limit. These intervening and undetected metabolites are colored grey in the metabolic network. The network shows the TCA cycle as the central pathway where common metabolites connect the urea cycle, alanine metabolism, and glycolysis/gluconeogenesis that then leads to amino sugar metabolism and other metabolites associated with PIA synthesis.

Conclusion

The systematic analysis of the *S. epidermidis* metabolome using NMR provides further evidence for a metabolic signaling network for biofilm formation that involves the TCA cycle. Inactivation of the TCA cycle enables metabolic precursors to flow into pathways associated with PIA synthesis, an important component of *S. epidermidis* biofilm formation. Disparate environmental stress conditions known to induce biofilm formation were shown to perturb the metabolome of *S. epidermidis* in a manner similar to an aconitase mutant. Effectively, iron-depletion, and the addition of ethanol, tetracycline, and glucose resulted in the inactivation of the TCA cycle. Furthermore, a detailed analysis of the specific changes to the *S. epidermidis* metabolome indicates that essentially the same set of metabolites affected by TCA cycle inactivation are also affected by environmental stress conditions. A network map identified the TCA cycle as playing a central role in the proposed signaling pathway that also involves the urea cycle, alanine metabolism, glycolysis/gluconeogenesis, amino sugar metabolism and other metabolites associated with PIA synthesis. Interestingly, the addition of NaCl or autoinducer-2 did not induce any effect on the *S. epidermidis* metabolome or effect TCA cycle activity. Suggesting these factors must act through a distinct process from the other environmental factors.

Supplementary Material

Refer to Web version on PubMed Central for supplementary material.

Acknowledgments

This manuscript is a contribution of the University of Nebraska Agricultural Research Division, supported in part by funds provided through the Hatch Act and from the National Institute of Health to G. A. S. (AI087668), from the NIH National Center for Research Resources to R. P. (P20 RR-17675), and from the American Heart Association to R. P. (0860033Z). The research was performed in facilities renovated with support from NIH (RR015468-01).

References

1. Brent R. Cell signaling: What is the signal and what information does it carry. FEBS Lett. 2009; 583(24):4019–4024. [PubMed: 19917282]
2. Jorgensen C, Linding R. Simplistic pathways or complex networks? Curr Opin Genet Dev. 2010; 20(1):15–22. [PubMed: 20096559]
3. Kholodenko BN. Spatially distributed cell signaling. FEBS Lett. 2009; 583(24):4006–4012. [PubMed: 19800332]
4. Scott JD, Pawson T. Cell signaling in space and time: Where proteins come together and when they're apart. Science. 2009; 326(5957):1220–1224. [PubMed: 19965465]
5. Mascher T, Helmann JD, Unden G. Stimulus perception in bacterial signal-transducing histidine kinases. Microbiol Mol Biol Rev. 2006; 70(4):910–938. [PubMed: 17158704]
6. Gill SR, Fouts DE, Archer GL, Mongodin EF, DeBoy RT, Ravel J, Paulsen IT, Kolonay JF, Brinkac L, Beanan M, Dodson RJ, Daugherty SC, Madupu R, Angiuoli SV, Durkin AS, Haft DH, Vamathevan J, Khouri H, Utterback T, Lee C, Dimitrov G, Jiang L, Qin H, Weidman J, Tran K, Kang K, Hance IR, Nelson KE, Fraser CM. Insights on evolution of virulence and resistance from the complete genome analysis of an early methicillin-resistant *Staphylococcus aureus* strain and a biofilm-producing methicillin-resistant *Streptococcus epidermidis* strain. J Bacteriol. 2005; 187(7): 2426–2438. [PubMed: 15774886]
7. Novick RP, Geisinger E. Quorum sensing in staphylococci. Annu Rev Genet. 2008; 42(1):541–564. [PubMed: 18713030]
8. Reznikoff WS, Siegele DA, Cowing DW, Gross CA. The regulation of transcription initiation in bacteria. Annu Rev Genet. 1985; 19:355–87. [PubMed: 3936407]
9. Wu S, de LH, Tomasz A. Sigma-B, a putative operon encoding alternate sigma factor of *Staphylococcus aureus* RNA polymerase: molecular cloning and DNA sequencing. J Bacteriol. 1996; 178(20):6036–6042. [PubMed: 8830703]
10. Senn MM, Giachino P, Homerova D, Steinhuber A, Strassner J, Kormanec J, Fluckiger U, Berger-Bachi B, Bischoff M. Molecular analysis and organization of the σ^B operon in*Staphylococcus aureus*. J Bacteriol. 2005; 187(23):8006–8019. [PubMed: 16291674]
11. Somerville GA, Proctor RA. At the crossroads of bacterial metabolism and virulence factor synthesis in Staphylococci. Microbiol Mol Biol Rev. 2009; 73(2):233–248. [PubMed: 19487727]
12. Lloyd D. The tricarboxylic acid cycle. Process Biochem. 1966; 1(9):465–9.
13. Bae T, Banger AK, Wallace A, Glass EM, Aslund F, Schneewind O, Missiakas DM. *Staphylococcus aureus* virulence genes identified by *bursa aurealis* mutagenesis and nematode killing. Proc Natl Acad Sci U S A. 2004; 101(33):12312–7. [PubMed: 15304642]
14. Begun J, Sifri CD, Goldman S, Calderwood SB, Ausubel FM. *Staphylococcus aureus* virulence factors identified by using a high-throughput *Caenorhabditis elegans*-killing model. Infect Immun. 2005; 73(2):872–7. [PubMed: 15664928]
15. Coulter SN, Schwan WR, Ng EY, Langhorne MH, Ritchie HD, Westbrock-Wadman S, Hufnagle WO, Folger KR, Bayer AS, Stover CK. *Staphylococcus aureus* genetic loci impacting growth and survival in multiple infection environments. Mol Microbiol. 1998; 30(2):393–404. [PubMed: 9791183]

16. Sadykov MR, Olson ME, Halouska S, Zhu Y, Fey PD, Powers R, Somerville GA. Tricarboxylic acid cycle-dependent regulation of *Staphylococcus epidermidis* polysaccharide intercellular adhesin synthesis. J Bacteriol. 2008; 190(23):7621–32. [PubMed: 18820013]

17. Cramton SE, Gerke C, Schnell NF, Nichols WW, Gotz F. The intercellular adhesion (*ica*) locus is present in *Staphylococcus aureus* and is required for biofilm formation. Infect Immun. 1999; 67(10):5427–33. [PubMed: 10496925]

18. Maira-Litran T, Kropec A, Abeygunawardana C, Joyce J, Mark G 3rd, Goldmann DA, Pier GB. Immunochemical properties of the staphylococcal poly-N-acetylglucosamine surface polysaccharide. Infect Immun. 2002; 70(8):4433–40. [PubMed: 12117954]

19. Rupp ME, Ulphani JS, Fey PD, Bartscht K, Mack D. Characterization of the importance of polysaccharide intercellular adhesin/hemagglutinin of *Staphylococcus epidermidis* in the pathogenesis of biomaterial-based infection in a mouse foreign body infection model. Infect Immun. 1999; 67(5):2627–32. [PubMed: 10225932]

20. Rupp ME, Ulphani JS, Fey PD, Mack D. Characterization of *Staphylococcus epidermidis* polysaccharide intercellular adhesin/hemagglutinin in the pathogenesis of intravascular catheter-associated infection in a rat model. Infect Immun. 1999; 67(5):2656–9. [PubMed: 10225938]

21. Fitzpatrick F, Humphreys H, O'Gara JP. The genetics of staphylococcal biofilm formation--will a greater understanding of pathogenesis lead to better management of device-related infection. Clin Microbiol Infect. 2005; 11(12):967–73. [PubMed: 16307550]

22. Vuong C, Kidder JB, Jacobson ER, Otto M, Proctor RA, Somerville GA. *Staphylococcus epidermidis* polysaccharide intercellular adhesin production significantly increases during tricarboxylic acid cycle stress. J Bacteriol. 2005; 187(9):2967–73. [PubMed: 15838022]

23. Sadykov MR, Zhang B, Halouska S, Nelson JL, Kreimer LW, Zhu Y, Powers R, Somerville GA. Using NMR metabolomics to investigate tricarboxylic acid cycle dependent signal transduction in*Staphylococcus epidermidis*. J Biol Chem. 2010; 285(47):36616–24. [PubMed: 20861019]

24. Knobloch JKM, Bartscht K, Sabottke A, Rohde H, Feucht HH, Mack D. Biofilm formation by *Staphylococcus epidermidis* depends on functional RsbU, an activator of the *sigB* operon: Differential activation mechanisms due to ethanol and salt stress. J Bacteriol. 2001; 183(8):2624–2633. [PubMed: 11274123]

25. Campbell IM, Crozier DN, Pawagi AB, Buivids IA. *In vitro* response of *Staphylococcus aureus* from cystic fibrosis patients to combinations of linoleic and oleic acids added to nutrient medium. J Clin Microbiol. 1983; 18(2):408–15. [PubMed: 6619290]

26. Mack D, Siemssen N, Laufs R. Parallel induction by glucose of adherence and a polysaccharide antigen specific for plastic-adherent *Staphylococcus epidermidis*: evidence for functional relation to intercellular adhesion. Infect Immun Infect Immun. 1992; 60(5):2048–57.

27. Gerke C, Kraft A, Sussmuth R, Schweitzer O, Gotz F. Characterization of the N-acetylglucosaminyltransferase activity involved in the biosynthesis of the *Staphylococcus epidermidis* polysaccharide intercellular adhesin. J Biol Chem. 1998; 273(29):18586–18593. [PubMed: 9660830]

28. Rachid S, Ohlsen K, Witte W, Hacker J, Ziebuhr W. Effect of subinhibitory antibiotic concentrations on polysaccharide intercellular adhesin expression in biofilm-forming*Staphylococcus epidermidis*. Antimicrob Agents Chemother. 2000; 44(12):3357–63. [PubMed: 11083640]

29. Cramton SE, Ulrich M, Gotz F, Doring G. Anaerobic conditions induce expression of polysaccharide intercellular adhesin in *Staphylococcus aureus* and*Staphylococcus epidermidis*. Infect Immun. 2001; 69(6):4079–85. [PubMed: 11349079]

30. Deighton M, Borland R. Regulation of slime production in *Staphylococcus epidermidis* by iron limitation. Infect Immun. 1993; 61(10):4473–9. [PubMed: 8406839]

31. Elci S, Atmaca S, Gul K. Effect of iron limitation on the amount of slime produced by strains of*Staphylococcus epidermidis*. Cytobios. 1995; 84:338–339. 141–6.

32. Evans E, Brown MRW, Gilbert P. Iron chelator, exopolysaccharide and protease production in *Staphylococcus epidermidis*: a comparative study of the effects of specific growth rate in biofilm and planktonic culture. Microbiology. 1994; 140(1):153–7. [PubMed: 8162184]

33. Rachid S, Ohlsen K, Wallner U, Hacker J, Hecker M, Ziebuhr W. Alternative transcription factor σ^B is involved in regulation of biofilm expression in a *Staphylococcus aureus* mucosal isolate. J Bacteriol. 2000; 182(23):6824–6. [PubMed: 11073930]
34. Zhao L, Xue T, Shang F, Sun H, Sun B. *Staphylococcus aureus* AI-2 quorum sensing associates with the KdpDE two-component system to regulate capsular polysaccharide synthesis and virulence. Infect Immun. 2010; 78(8):3506–3515. [PubMed: 20498265]
35. Forgue P, Halouska S, Werth M, Xu K, Harris S, Powers R. NMR metabolic profiling of *aspergillus nidulans* to monitor drug and protein activity. J Proteome Res. 2006; 5(8):1916–1923. [PubMed: 16889413]
36. Halouska S, Chacon O, Fenton RJ, Zinniel DK, Barletta RG, Powers R. Use of NMR metabolomics to analyze the targets of D-cycloserine in mycobacteria: role of D-alanine racemase. J Proteome Res. 2007; 6(12):4608–4614. [PubMed: 17979227]
37. Werth MT, Halouska S, Shortridge MD, Zhang B, Powers R. Analysis of metabolomic pca data using tree diagrams. Anal Biochem. 2010; 399(1):56–63.
38. Lindon JC, Holmes E, Nicholson JK. Pattern recognition methods and applications in biomedical magnetic resonance. Prog Nucl Magn Reson Spectrosc. 2001; 39(1):40.
39. Stoyanova R, Brown TR. NMR spectral quantitation by principal component analysis. NMR Biomed. 2001; 14(4):271–7. [PubMed: 11410945]
40. Killcoyne S, Carter GW, Smith J, Boyle J. Cytoscape: a community-based framework for network modeling. Methods Mol Biol. 2009; 563:219–39. [PubMed: 19597788]
41. Cao JG, Meighen EA. Purification and structural identification of an autoinducer for the luminescence system of Vibrio harveyi. J Biol Chem. 1989; 264(36):21670–6. [PubMed: 2600086]
42. Semmelhack MF, Campagna SR, Federle MJ, Bassler BL. An Expeditious Synthesis of DPD and Boron Binding Studies. Org Lett. 2005; 7(4):569–572. [PubMed: 15704896]
43. Nguyen BD, Meng X, Donovan KJ, Shaka AJ. SOGGY: solvent-optimized double gradient spectroscopy for water suppression. A comparison with some existing techniques. J Magn Reson. 2007; 184(2):263–74. [PubMed: 17126049]
44. Palmer AG III, Cavanagh J, Wright PE, Rance MJ. Sensitivity improvement in proton-detected two-dimensional heteronuclear correlation NMR spectroscopy. J Magn Reson. 1991; 93(1):20.
45. Kay LE, Keifer P, Saarinen T. Pure absorption gradient enhanced heteronuclear single quantum correlation spectroscopy with improved sensitivity. J Am Chem Soc. 1992; 114(26):3.
46. Bax A, Davis DG. MLEV-17-based two-dimensional homonuclear magnetization transfer spectroscopy. J Magn Reson. 1985; 65:6.
47. Piotto M, Saudek V, Sklenar V. Gradient-tailored excitation for single-quantum NMR spectroscopy of aqueous solutions. J Biomol NMR. 1992; 2(6):661–5. [PubMed: 1490109]
48. Halouska S, Powers R. Negative impact of noise on the principal component analysis of NMR data. J Magn Reson. 2006; 178(1):88–95. [PubMed: 16198132]
49. Johnson BA. Using NMRView to visualize and analyze the NMR spectra of macromolecules. Methods Mol Biol. 2004; 278:313–52. [PubMed: 15318002]
50. Xia J, Bjorndahl TC, Tang P, Wishart DS. Metabominer-semi-automated identification of metabolites from 2D NMR spectra of complex biofluids. BMC Bioinf. 2008; 9 No pp. given.
51. Cui Q, Lewis IA, Hegeman AD, Anderson ME, Li J, Schulte CF, Westler WM, Eghbalnia HR, Sussman MR, Markley JL. Metabolite identification via the Madison Metabolomics Consortium Database. Nat Biotechnol. 2008; 26(2):162–4. [PubMed: 18259166]
52. Ulrich EL, Akutsu H, Doreleijers JF, Harano Y, Ioannidis YE, Lin J, Livny M, Mading S, Maziuk D, Miller Z, Nakatani E, Schulte CF, Tolmie DE, Kent WR, Yao H, Markley JL. BioMagResBank. Nucleic Acids Res. 2008; 36(Database Iss):D402–408. [PubMed: 17984079]
53. Wishart DS, Knox C, Guo AC, Eisner R, Young N, Gautam B, Hau DD, Psychogios N, Dong E, Bouatra S, Mandal R, Sinelnikov I, Xia J, Jia L, Cruz JA, Lim E, Sobsey CA, Shrivastava S, Huang P, Liu P, Fang L, Peng J, Fradette R, Cheng D, Tzur D, Clements M, Lewis A, De SA, Zuniga A, Dawe M, Xiong Y, Clive D, Greiner R, Nazyrova A, Shaykhutdinov R, Li L, Vogel HJ, Forsythe I. HMDB: a knowledge-base for the human metabolome. Nucleic Acids Res. 2009; 37(Database Iss):D603–610. [PubMed: 18953024]

54. Kanehisa M, Araki M, Goto S, Hattori M, Hirakawa M, Itoh M, Katayama T, Kawashima S, Okuda S, Tokimatsu T, Yamanishi Y. KEGG for linking genomes to life and the environment. Nucleic Acids Res. 2008; 36(Database Iss):D480–484. [PubMed: 18077471]
55. Caspi R, Altman T, Dale JM, Dreher K, Fulcher CA, Gilham F, Kaipa P, Karthikeyan AS, Kothari A, Krummenacker M, Latendresse M, Mueller LA, Paley S, Popescu L, Pujar A, Shearer AG, Zhang P, Karp PD. The MetaCyc database of metabolic pathways and enzymes and the BioCyc collection of pathway/genome databases. Nucleic Acids Res. 2010; 38(Database Iss):D473–479. [PubMed: 19850718]
56. van den Berg RA, Hoefsloot HC, Westerhuis JA, Smilde AK, van der Werf MJ. Centering, scaling, and transformations: improving the biological information content of metabolomics data. BMC Genomics. 2006; 7:142. [PubMed: 16762068]
57. Somerville GA, Chaussee MS, Morgan CI, Fitzgerald JR, Dorward DW, Reitzer LJ, Musser JM. *Staphylococcus aureus* aconitase inactivation unexpectedly inhibits post-exponential-phase growth and enhances stationary-phase survival. Infect Immun. 2002; 70(11):6373–6382. [PubMed: 12379717]
58. Mack D, Becker P, Chatterjee I, Dobinsky S, Knobloch JKM, Peters G, Rohde H, Herrmann M. Mechanisms of biofilm formation in *Staphylococcus epidermidis* and *Staphylococcus aureus*: Functional molecules, regulatory circuits, and adaptive responses. Int J Med Microbiol. 2004; 294:2–3. 203–212.
59. Collins FM, Lascelles J. The effect of growth conditions on oxidative and dehydrogenase activity in*Staphylococcus aureus*. J Gen Microbiol. 1962; 29:531–5. [PubMed: 14022366]
60. Costerton JW, Stewart PS, Greenberg EP. Bacterial biofilms: a common cause of persistent infections. Science. 1999; 284(5418):1318–22. [PubMed: 10334980]
61. Kornmann H, Duboc P, Niederberger P, Marison I, von Stockar U. Influence of residual ethanol concentration on the growth of *Gluconacetobacter xylinus* I 2281. Appl Microbiol Biotechnol. 2003; 62:2–3. 168–73.
62. Throup JP, Zappacosta F, Lunsford RD, Annan RS, Carr SA, Lonsdale JT, Bryant AP, McDevitt D, Rosenberg M, Burnham MK. The *srhSR* gene pair from *Staphylococcus aureus*: genomic and proteomic approaches to the identification and characterization of gene function. Biochemistry. 2001; 40(34):10392–401. [PubMed: 11513618]
63. Tomlins RI, Pierson MD, Ordal ZJ. Effect of thermal injury on the TCA cycle enzymes of *Staphylococcus aureus* MF 31 and Salmonella typhimurium 7136. Can J Microbiol. 1971; 17(6): 759–65. [PubMed: 4932097]
64. Miller MB, Bassler BL. Quorum sensing in bacteria. Annu Rev Microbiol. 2001; 55:165–199. [PubMed: 11544353]
65. Lim Y, Jana M, Luong TT, Lee CY. Control of glucose- and NaCl-induced biofilm formation by rbf in*Staphylococcus aureus*. J Bacteriol. 2004; 186(3):722–9. [PubMed: 14729698]
66. Cue D, Lei MG, Luong TT, Kuechenmeister L, Dunman PM, O'Donnell S, Rowe S, O'Gara JP, Lee CY. Rbf promotes biofilm formation by *Staphylococcus aureus* via repression of *icaR*, a negative regulator of*icaADBC*. J Bacteriol. 2009; 191(20):6363–6373. [PubMed: 19684134]
67. Heilmann C, Schweitzer O, Gerke C, Vanittanakom N, Mack D, Goetz F. Molecular basis of intercellular adhesion in the biofilm-forming*Staphylococcus epidermidis*. Mol Microbiol. 1996; 20(5):1083–1091. [PubMed: 8809760]
68. Hoffman LR, D'Argenio DA, MacCoss MJ, Zhang Z, Jones RA, Miller SI. Aminoglycoside antibiotics induce bacterial biofilm formation. Nature. 2005; 436(7054):1171–1175. [PubMed: 16121184]
69. Chang YM, Jeng WY, Ko TP, Yeh YJ, Chen CKM, Wang AHJ. Structural study of TcaR and its complexes with multiple antibiotics from*Staphylococcus epidermidis*. Proc Natl Acad Sci U S A. 2010; 107(19):8617–8622. S8617/1–8617/13. [PubMed: 20421503]
70. Sousa C, Henriques M, Azeredo J, Teixeira P, Oliveira R. *Staphylococcus epidermidis* glucose uptake in biofilm versus planktonic cells. World J Microbiol Biotechnol. 2008; 24(3):423–426.
71. Croes S, Deurenberg RH, Boumans MLL, Beisser PS, Neef C, Stobberingh EE. *Staphylococcus aureus* biofilm formation at the physiologic glucose concentration depends on the *S. aureus* lineage. BMC Microbiol. 2009; 9 Epub.

72. Somerville GA, Said-Salim B, Wickman JM, Raffel SJ, Kreiswirth BN, Musser JM. Correlation of acetate catabolism and growth yield in *Staphylococcus aureus*: implications for host-pathogen interactions. Infect Immun. 2003; 71(8):4724–32. [PubMed: 12874354]

73. Cline MS, Smoot M, Cerami E, Kuchinsky A, Landys N, Workman C, Christmas R, Avila-Campilo I, Creech M, Gross B, Hanspers K, Isserlin R, Kelley R, Killcoyne S, Lotia S, Maere S, Morris J, Ono K, Pavlovic V, Pico AR, Vailaya A, Wang PL, Adler A, Conklin BR, Hood L, Kuiper M, Sander C, Schmulevich I, Schwikowski B, Warner GJ, Ideker T, Bader GD. Integration of biological networks and gene expression data using Cytoscape. Nat Protoc. 2007; 2(10):2366–82. [PubMed: 17947979]

74. Shannon P, Markiel A, Ozier O, Baliga NS, Wang JT, Ramage D, Amin N, Schwikowski B, Ideker T. Cytoscape: a software environment for integrated models of biomolecular interaction networks. Genome Res. 2003; 13(11):2498–504. [PubMed: 14597658]

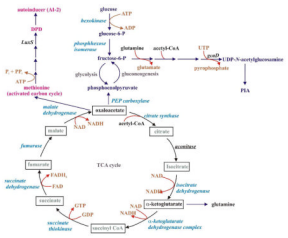

Figure 1.
An illustration of the interrelationship of metabolic pathways associated with the TCA cycle and biofilm formation.

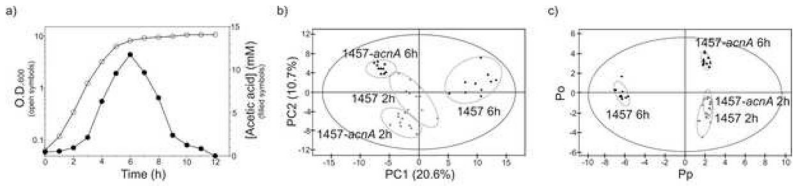

Figure 2.

a) A typical *S. epidermidis* growth curve superimposed on the cellular production of acetic acid. b) 2D PCA scores plot and c) 2D OPLS-DA scores plot comparing 2 h growth of wild-type *S. epidermidis* 1457 (●), 2 h growth of aconitase mutant strain 1457-*acnA::tet*M (▲), 6 h growth of wild-type *S. epidermidis* 1457 (●), and 6 h growth of aconitase mutant strain 1457-*acnA::tet*M (▲). The ellipses correspond to the 95% confidence limits from a normal distribution for each cluster. For the OPLS-DA scores plot, the 6 h growth of wild-type *S. epidermidis* 1457 (●) was designated the control class and the remainder of the cells were designated as treated. The OPLS-DA used 1 predictive component and 3 orthogonal components to yield a R^2X of 0.788, R^2Y of 0.992 and Q^2 of 0.992.

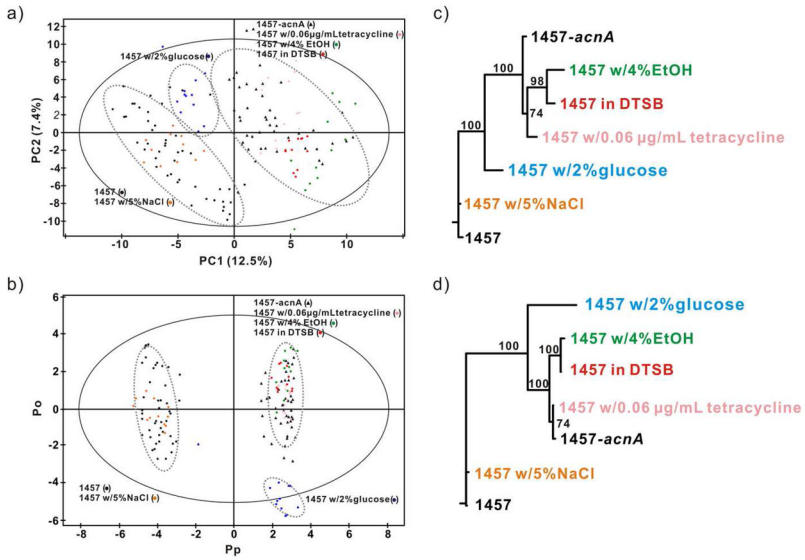

Figure 3.

a) 2D PCA scores plot and b) 2D OPLS-DA comparing wild-type *S. epidermidis* 1457 cells grown 6 h in standard TSB media (●), with *S. epidermidis* 1457 cells grown 6 h in iron-depleted media (DTSB) (●), with the addition of 4% ethanol (●), with the addition of 2% glucose (●), with the addition of 0.06 µg/mL tetracycline (●), with the addition of 5% NaCl (●), and 6 h growth of aconitase mutant strain 1457-*acnA::tet*M in standard TSB media (▲). The ellipses correspond to the 95% confidence limits from a normal distribution for each cluster. For the OPLS-DA scores plot, the 6 h growth of wild-type *S. epidermidis* 1457 (●) was designated the control class and the remainder of the cells were designated as treated. The OPLS-DA used 1 predictive component and 4 orthogonal components to yield a R^2X of 0.637, R^2Y of 0.966 and Q^2 of 0.941. Metabolomic tree diagram generated from the c) 2D PCA scores plot depicted in (a) and d) 2D OPLS-DA scores plot depicted in (b). The label colors match the symbol colors from the 2D scores plot. Each node is labeled with the boot-strap number, where a value above 50 indicates a statistically significant separation.

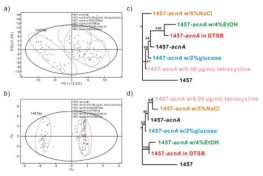

Figure 4.

a) 2D PCA scores plot and b) 2D OPLS-DA comparing wild-type *S. epidermidis* 1457 cells grown 6 h in standard TSB media (●), 6 h growth of aconitase mutant strain 1457-*acnA::tet*M in standard TSB media (▲), aconitase mutant strain 1457-*acnA::tet*M in iron-depleted media (DTSB) (▲), with the addition of 4% ethanol (▲), with the addition of 2% glucose (▲), with the addition of 0.06 μg/mL tetracycline (▲), and with the addition of 5% NaCl (▲). The ellipses correspond to the 95% confidence limits from a normal distribution for each cluster. The four ellipses correspond to clusters formed by (i) wild-type *S. epidermidis* 1457 cells, (ii) aconitase mutant strain 1457-*acnA::tet*M in standard TSB media, (iii) aconitase mutant strain 1457-*acnA::tet*M in DTSB or with the addition of 4% ethanol, and (iv), aconitase mutant strain 1457-*acnA::tet*M with the addition of 2% glucose, 0.06 μg/mL tetracycline, or 5% NaCl. For the OPLS-DA scores plot, the 6 h growth of wild-type *S. epidermidis* 1457 (●) was designated the control class and the remainder of the cells were designated as treated. The OPLS-DA used 1 predictive component and 2 orthogonal components to yield a R^2X of 0.488, R^2Y of 0.976 and Q^2 of 0.961. Metabolomic tree diagram generated from the c) 2D PCA scores plot depicted in (a) and d) 2D OPLS-DA scores plot depicted in (b). The label colors match the symbol colors from the 2D scores plot. Each node is labeled with the boot-strap number, where a value above 50 indicates a statistically significant separation.

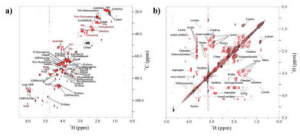

Figure 5.
Overlay of (a) 2D ^{1}H-^{13}C HSQC spectra and (b) 2D ^{1}H-^{1}H TOCSY spectra comparing wild-type *S. epidermidis* strain 1457 (red) and aconitase mutant strain 1457-*acnA::tet*M (black) grown for 6 h in standard TSB media augmented with 0.25% ^{13}C-glucose. NMR resonances corresponding to specific metabolites are labeled, where citrate is circled.

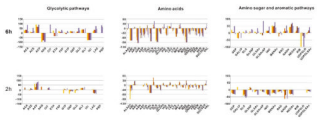

Figure 6.

Bar graphs showing the percent change in metabolite concentrations relative to wild-type *S. epidermidis* strain 1457 grown in standard TSB media. Metabolite concentration changes were measured after 2 h and 6 h bacterial growths for the aconitase mutant strain 1457-*acnA::tet*M in TSB media ( ), aconitase mutant strain 1457-*acnA::tet*M with iron-depletion ( ), aconitase mutant strain 1457-*acnA::tet*M with the addition of 4% ethanol ( ), wild-type *S. epidermidis* strain 1457 with iron-depletion ( ), and wild-type *S. epidermidis* strain 1457 with the addition of 4% ethanol ( ) Positive values represent increased concentrations while negative values represent decreased concentrations with respect to *S. epidermidis* strain 1457 grown in standard TSB media. The metabolite names were abbreviated as follows: ACA (Acetaldehyde), ACE (Acetate), ACP (Acetyl-P), AKG (α-ketoglutarate), ALAAc (Acetyl-alanine), AMI (4-Aminobutanoate), ARG (Arginine), ASN (Asparagine), ASP (Aspartate), CIR (Citrulline), CIT (Citrate), ETH (Ethanol), F6P (Fruc-6P), G1P (Gluc-1P), G6P (Gluc-6P), GAL (Galacturonic-acid), GAL1P (α-D-Gala-1P), GLN (Glutamine), GLR (Glucuronate), GLS (D-glucosamine), GLS6P (Glucosamine-6P), GLSAc (N-Ac-D-glucosamine), GLSAc6P (Acetyl-glucosamine-6P), GLU (Glutamate), GLUAc (Acetyl-glutamate), GLY (Glyceraldehyde), HIS (Histidine), ICI (Isocitrate), INO (Ino, Ade, Xan), LAC (Lactate), ALA (alanine), LEU (Leucine), LYS (Lysine), MANAc (N-acetyl-D-mannosamine), MET (Methionine), MIN (myo inositol), MSE (selenomethionine), NEUAc (N-Ac-neuraminate), ORN (Ornithine), ORNAc (Acetyl-ornithine), PEP (Phosphoenolpyruvic acid), PRO (Proline), RIB (D-ribose), SAM(S-adenosyl-methionine), SER (Homoserine), SUCSER (O-Succinyl-L-homoserine), UDPGLR (UDP-glucoronate), UDPGLSAc (UDP-NAc-D-glucosamine), VAL (Valine)

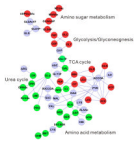

Figure 7.
Cytoscape[40] network depicting the metabolite concentration changes caused by the inactivation of the TCA cycle. Nodes colored red correspond to metabolites with an increase in concentration due to TCA inactivated. Nodes colored green correspond to metabolites with a decrease in concentration due to TCA inactivated. Nodes colored grey correspond to metabolites that are not observed in the NMR spectra, do not have a reference NMR spectrum (or assignment), or did not exhibit a significant concentration change. Metabolic pathways are labeled on the network. The metabolite names were abbreviated as described in the legend to Figure 6.